Macromolecules
ARTICLE

Macromolecules **2009**, *42*, 8543–8556 **8543**
DOI: 10.1021/ma901536e

Soft Confinement in Spherical Mesophases of Block Copolymer Melts

Angel J. Moreno*,† and Juan Colmenero†,‡,§

†*Centro de Física de Materiales (CSIC, UPV/EHU)-Materials Physics Center, Apartado 1072, 20080 San Sebastián, Spain,* ‡*Donostia International Physics Center, Paseo Manuel de Lardizabal 4, 20018 San Sebastián, Spain, and* §*Departamento de Física de Materiales, Universidad del País Vasco (UPV/EHU), Apartado 1072, 20080 San Sebastián, Spain*

Received July 15, 2009; Revised Manuscript Received September 11, 2009

ABSTRACT: We report an extensive computational investigation on the dynamics of a simple bead−spring model for melts of diblock (AB) copolymers. Monomer displacements, end-to-end and bond reorientations, as well as relaxation of chain normal modes, are characterized both in the homogeneous phase and in the limit of strong segregation. In the latter case, the B-blocks are aggregated into "micellar-like" spherical domains. We investigate the case in which the B-homopolymer exhibits a much higher glass transition temperature than the A-homopolymer, and thus an intrinsically much slower mobility. In such conditions, the interplay between a strong interfacial barrier suppressing diffusion and a highly mobile surrounding corona induces a soft confinement effect on the B-blocks forming the spherical cores. The spontaneously formed spherical phase is highly polydisperse in the micellar aggregation number. However, this is a minor source of dynamic heterogeneity in comparison to the specific location of the monomer along the chain. The time scales for bond reorientation exhibit extreme differences between bonds close to the micellar interface and those close to the chain ends. The comparison of orientational correlators and normal modes for the B-component in the diblock system and in the homopolymer state reveals scaling behavior. Results are rationalized within the Rouse model, for intermediate time scales not probing the interface, through a change in the effective friction with the temperature and the energy scale of the A−B interaction.

I. Introduction

Self-assembly of block copolymers is one of the most active fields of research in soft matter systems.[1−6] In concentrate solutions and melt states, block copolymers of thermodynamically immiscible components can exhibit microphase separation into domains rich in one component and poor in the other. These domains can be arranged in ordered periodic structures. The transition from the disordered to the ordered state and between the different ordered mesophases can be easily tuned by changing control parameters as temperature, chain length, or monomer fraction of each component. For the most simple case of diblock copolymers, the equilibrium ordered phases include,[1−9] for increasing asymmetry in the composition, planar lamellae, hexagonal arrays of cylinders, and bcc lattices of "micellar-like" spherical domains (in the following, we will refer to the spherical domains as "micelles"). A bicontinuous gyroid structure[10] can also exist in reduced regions of the phase diagram between the lamellar and cylinder phases. Ordered mesophases of block copolymers have numerous advanced technological applications,[11] as membranes, photonic materials or templates for nanostructured systems.

Much of the theoretical and experimental effort dedicated to block copolymers have focused on their phase behavior and structural properties (see, e.g., the extensive reviews in refs 1, 7, 8, and 12). Concerning dynamic features of diblock copolymers,[13−16] most of the investigations in inhomogenous phases have focused on the lamellar structure.[17−34] A general observation around the order−disorder transition is a bifurcation of the diffusivity into two components parallel and perpendicular to the lamellar planes. It is worthy of remark that this bifurcation is apparently not accompanied by a discontinuity in the diffusivity around the order−disorder transition. For the case of nonentangled chains, diffusion in the lamellar phase is strongly anisotropic, with a strong reduction of the perpendicular component.[18,27−29] On the other hand, for entangled chains differences between perpendicular and parallel diffusivities are strongly reduced.[19,20,22,30] Concerning the local orientational relaxation in the mobile block of lamellar phases with large dynamic separation between the two components, strong dynamic heterogeneity (gradient of mobility) is usually invoked to understand the observed broad distributions of relaxation times[33].

Dynamic features in cylinder,[23,35−37] gyroid,[31,35] and spherical micellar phases[38−45] have received much less attention. In the spherical case the interface forms a finite closed surface for the minority component. The interfacial barrier induces a dramatic reduction of the total diffusivity D in comparison to that in the absence of any interactions, D_0. Thus, the ratio D/D_0 shows an exponential reduction by increasing the chain length and the energy scale of the cross-interaction.[39,41,42,44,45] In this situation, the minority blocks are confined within the micellar cores for extremely long time scales, and chain diffusion esentially occurs through hopping events with large activation energies.

Because of the long time scales involved for global diffusion (in spherical micellar phases) or for diffusion along specific directions (in lamellar and cylinder phases), the dynamics in diblock copolymers at more local scales (including segmental dynamics and chain end-to-end reorientation) show connections with the problem of dynamics in confined systems. When the two homopolymers forming the diblock exhibit similar intrinsic mobilities (i.e., similar glass transition temperatures), the coupling between the two blocks in the *homogeneous* phase is not expected to induce relaxation time scales very different from

*Corresponding author. E-mail: wabmosea@ehu.es.

Published on Web 09/30/2009

those of the homopolymers. Thus, one expects that in the *inhomogeneous* segregated phase, dynamic differences with the homopolymer state are esentially driven by the interfacial barrier and/or confinement effects.

A different situation can be found if the two components have very different glass transition temperatures in the homopolymer state, and in particular for spherical phases in which the fast and slow component correspond respectively to the micellar corona and core. In this case one may expect that the large difference in the intrinsic mobilities of the two components plays an additional role. Strong fluctuations of the interface are now expected due to the high mobility of the corona monomers, so that the monomers at the core experience a sort of "soft" confinement, different from the usual "hard" confinement induced by static walls or stiff interfaces.

A realization of this physical picture has been obtained by Lund and co-workers[46], in recent experiments by dielectric spectroscopy on melts of asymmetric diblocks of poly-(isoprene)-poly(dimethylsiloxane) (PI−PDMS). In the investigated ordered phases the PI- and PDMS-blocks form respectively the micellar core and corona. The glass transition temperatures of the corresponding homopolymers are $T_g \approx 207$ K for PI and $T_g \approx 147$ K for PDMS. As a consequence, the two homopolymers exhibit very different relaxation time scales (PI being much slower) at the temperatures of the experiment ($T \sim 240$ K). In the micellar phase the PI-blocks exhibit a faster time scale, in comparison to PI-homopolymers with the same molecular weight. This is the case both for the segmental α-relaxation and for the reorientation of the end-to-end vector.[46] The observed broader relaxation profile for the PI-blocks in the micellar phase also suggests a broader distribution of relaxation times in comparison to the PI-homopolymer.

In this article, we present a thorough characterization of local relaxation features associated with the former scenario of soft confinement. We have investigated, by means of molecular dynamics simulations, a simple bead−spring model for diblock copolymer melts in the disordered homogeneous and spherical micellar phases. In particular, we have simulated diblock systems for which the corresponding homopolymers show very different intrinsic mobilities. The slow and fast homopolymers correspond, in the diblock system, to the blocks forming respectively the micellar core and corona. In this way the general conditions of the micellar systems with soft confinement are mimiced in the present model. We compute correlators probing translational and orientational dynamics. The effect of the distance to the interface is characterized by investigating the dependence of the former correlators on the specific location of the monomers along the blocks. This analysis reveals a strong dynamic heterogeneity for bond reorientation. The role of the micellar size polydispersity on dynamic heterogeneity is also studied. Finally, we discuss the limits of applicability of the Rouse model for the blocks in the micellar cores. The analysis of the chain normal modes (Rouse modes) suggests that the Rouse model is still a good physical picture for intermediate time scales not probing the interface.

The article is organized as follows. In section II, we describe the investigated model and give simulation details. Static properties and dynamic correlators are presented respectively in sections III and IV. Dynamic features of the chain normal modes are discussed in section V. Conclusions are given in section VI.

II. Model and Simulation Details

We have performed molecular dynamics simulations of a system of $N_{cha} = 1050$ identical bead−spring diblock chains. The blocks consist of $N_A = 61$ A-monomers and $N_B = 9$ B-monomers. Thus, the fraction of B-monomers in the system is $f_B = 0.13$, for which a spherical micellar phase is expected in the ordered state.[1,7,8] For simplicity the mass of both types of monomer is set to $m = 1$. For comparison with the dynamics in the homopolymer case we have also simulated two pure systems of A- and B-chains. The A-homopolymer consists of 1205 chains of 61 A-monomers. For the highest investigated temperature $T = 0.22$, the B-homopolymer consists of 8167 chains of 9 B-monomers. The latter exhibits, at a same temperature, a much slower relaxation than the other investigated systems (see below). For this reason we use, for $T = 0.08$ and $T = 0.12$, smaller systems of 600 chains for the B-homopolymer. All simulations are performed at fixed density of monomers $\rho = 1.0$. This density in bead−spring models qualitatively corresponds to melt densities in real polymers[47].

The interaction between any two given monomers of the species α and $\beta \in \{AB\}$ is given by a shifted Lennard-Jones potential:

$$V_{\alpha\beta}(r) = 4\epsilon_{\alpha\beta}\left[\left(\frac{\sigma_{\alpha\beta}}{r}\right)^{12} - \left(\frac{\sigma_{\alpha\beta}}{r}\right)^{6} + \frac{1}{4}\right] \qquad (1)$$

for $r < r_c$ and $V_{\alpha\beta}(r) = 0$ for $r \geq r_c$. By taking a value $r_c = 2^{1/6}\sigma_{\alpha\beta}$, potential and forces are continuous at the cutoff distance. Moreover the potential is purely repulsive and has no local minima. Thus, for a pure system it drives dynamic arrest only through packing effects. In addition to the Lennard-Jones potential, two connected monomers in a same chain interact through a finitely extensible nonlinear elastic potential (FENE)[47]:

$$V_{\alpha\beta}^{FENE}(r) = -\epsilon_{\alpha\beta}K_F R_0^2 \ln\left[1 - \left(\frac{r}{R_0\sigma_{\alpha\beta}}\right)^2\right] \qquad (2)$$

with $K_F = 15$ and $R_0 = 1.5$. The sum of the potential (2) with such parameters and the potential (1) yields an effective potential between connected monomers which shows a sharp minimum at $r = 0.96\sigma_{\alpha\beta}$ and guarantees chain uncrossability.[47]

For simplicity we use identical interaction diameters $\sigma_{AA} = \sigma_{BB} = \sigma_{AB} = 1$. We use the energy scales $\epsilon_{AA} = 0.35$ and $\epsilon_{BB} = 1$ for the self-interactions of the two components. For these selected values, the two homopolymers show very different relaxation time scales at fixed density and temperature (see below). In other words, they have very different glass transition temperatures. In particular, the homopolymer forming the micellar core (B) exhibits a much slower dynamics than the homopolymer forming the micellar corona (A). We investigate dynamic features for different values of the cross-interaction energy scale, ϵ_{AB}, probing both the homogeneous and strongly segregated limits. Namely, we obtain an homogeneous phase for $\epsilon_{AB} = 0.5$, while for $\epsilon_{AB} = 2$ and 9, the system forms an inhomogeneous phase of spherical micelles (see below).

In the following, temperature T, monomer density ρ, time t and distance will be given respectively in units of ϵ/k_B (with k_B the Boltzmann constant), σ_{BB}^{-3}, $\sigma_{BB}(m/\epsilon_{BB})^{1/2}$, and σ_{BB}. Cubic periodic boundary conditions are implemented. Equations of motion are integrated in the velocity Verlet scheme[48]. For the diblock system and for the B-homopolymer we use a time step of $\delta t = 3 \times 10^{-3}$ at $T = 0.22$, and $\delta t = 4 \times 10^{-3}$ at $T = 0.12$ and 0.08. For the A-homopolymer we use $\delta t = 5 \times 10^{-4}$ at $T = 0.22$, and $\delta t = 1 \times 10^{-3}$ at $T = 0.12$ and 0.08. Computation time is reduced by using a linked-cell method[48] for calculation of interparticle distances within interaction ranges.

The system is prepared by placing and growing the chains randomly in the simulation cell, with a constraint that avoids initial overlap of monomers within distances $r < 0.8$. The initial monomer density is $\rho = 0.5$. Equilibration consists of a first run where the cell is rescaled periodically by a factor $0.99 < f < 1$

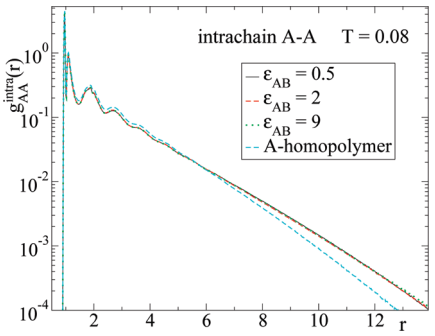

Figure 1. Radial distribution function for A−A intrachain correlations at $T = 0.08$. Data are given for the A-blocks, at all the investigated values of ϵ_{AB}, and for the A-homopolymer.

until the target density $\rho = 1.0$ is reached, and a second isochoric run at $\rho = 1.0$. Thermalization at the target temperature is achieved by periodic velocity rescaling. We consider that equilibration is reached when thermodynamic quantities as pressure or potential energy show no drift, and when relaxation of dynamic correlators does not depend on the selected time origin. Once the system is equilibrated, a microcanonical run is performed for production of configurations of the system, from which static and dynamic correlators are computed. For each state point, the latter are averaged over typically 20 equispaced time origins.

III. Static Properties

We compute radial distribution functions for static pair correlations. In a first step they are normalized so that their 3-dimensional integral over a sphere of radius R_s is equal to n_s/ρ_α. Here ρ_α is the macroscopic density of α-monomers, and n_s is the number of β-monomers within the former sphere, centered around an α-monomer (α, $\beta \in$ {A,B}), with the α−β pairs following the considered correlation (e.g., intrachain, interchain or total). Figure 1 shows results for the intrachain radial distribution function, $g_{AA}^{inta}(r)$, for correlations between pairs of A-monomers belonging to a same chain, and averaged over all the chains in the system. Data are shown for all the values of the cross-interaction energy ϵ_{AB}. Results for the A-homopolymer are also included for comparison. The normalization described above is not still adequate for a proper comparison between the homopolymer and the diblock system. This is only achieved after rescaling the $g_{AA}^{inta}(r)$ of the homopolymer (computed with the mentioned normalization) by a factor $(N_{cha}^{hom}N_A - 1)/(N_{cha}^{dib}N_A - 1)$, where N_{cha}^{hom} and N_{cha}^{dib} are respectively the number of chains in the homopolymer and diblock system. Numerical data in Figure 1 follow this procedure. The coupling between A- and B-blocks only induce weak perturbations of the correlations observed for the A-homopolymer (note the logarithmic scale in the ordinate axes of Figure 1). Namely, A-blocks exhibit stretching at large scales ($r \gtrsim 6$). The observed weak differences are consistent with the computed values of the average end-to-end radii of the A-blocks ($R_{ee} \approx 9.7$) and the corresponding A-homopolymers ($R_{ee} \approx 8.7$). Similarly, we have computed $g_{BB}^{inta}(r)$ (not shown). In this case differences between the B-blocks and the B-homopolymer are negligible.

Figure 2 shows results, for cross-interaction $\epsilon_{AB} = 0.5$ at different temperatures, of the interchain radial distribution functions $g_{AA}^{inter}(r)$, $g_{AB}^{inter}(r)$ and $g_{BB}^{inter}(r)$. The latter are computed for, respectively, A−A, A−B, and B−B correlations between monomers located at distinct chains. A rapid oscillatory decay to the limit $g_{\alpha\beta}^{inter}(r \to \infty) = 1$ is observed, as expected for a homogeneous phase with no long-range order. As usual, the growing of the first maximum by decreasing T is a signature of increasing order in the scale of nearest-neighbor distances. We also include

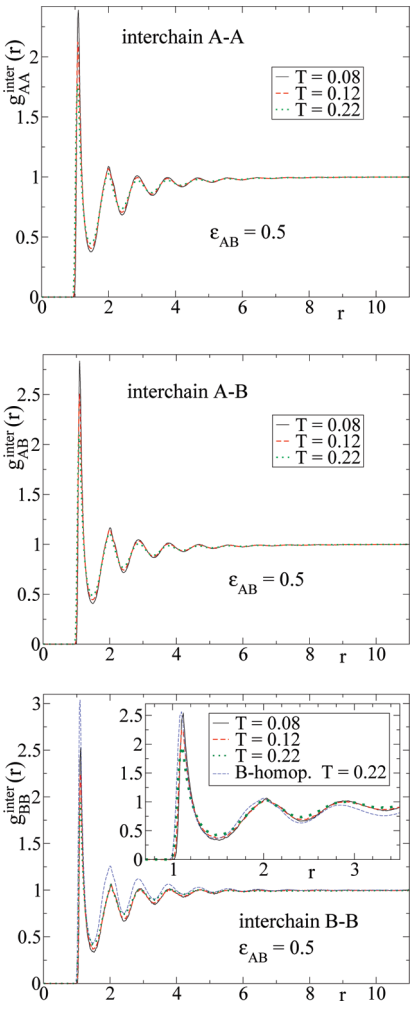

Figure 2. For $\epsilon_{AB} = 0.5$, T-dependence of radial distribution functions for interchain correlations (top, A−A; middle, A−B; bottom, B−B). The bottom panel also shows the corresponding results for the B-homopolymer at $T = 0.22$. The inset displays the same data sets at short distances, though now data for the B-homopolymer are rescaled for comparison with the diblock system at $T = 0.22$ (see text).

(bottom panel) the corresponding $g_{BB}^{inter}(r)$ for the B-homopolymer at $T = 0.22$. For an adequate comparison of short-ranged correlations in the homopolymer and the diblock system at the same $T = 0.22$, the inset in the bottom panel shows the same data for $r < 3.5$, but now $g_{BB}^{inter}(r)$ for the B-homopolymer is rescaled by a factor. This factor is so that the 3-dimensional integral of $g_{BB}^{inter}(r)$ from $r = 0$ to the second minimum becomes equal in the homopolymer and in the diblock. From this comparison, we observe that B−B interchain correlations of the homopolymer are just moderately perturbed, with increased disorder, in the homogeneous diblock phase.

Figure 3 shows the same functions of Figure 2 for the case $\epsilon_{AB} = 9$. Rather different features are observed. Thus, the interchain radial distribution functions $g_{AB}^{inter}(r)$ and $g_{BB}^{inter}(r)$ exhibit now strong oscillations of large wavelength (see the minima and maxima at $r \approx 9$ and $r \approx 16$), which are in antiphase for A−B and B−B correlations and do not decay within the simulation cell. This feature suggests a microphase separation into strongly segregated domains rich in A- or B-monomers. The absence of strong oscillations in $g_{AA}^{inter}(r)$ at long distances (see top panel) suggests that the A-domains form a connected structure, which strongly smooths the A−A correlation holes induced by the B-domains. Likewise, the results displayed for $g_{AB}^{inter}(r)$ and $g_{BB}^{inter}(r)$ suggest that the B-monomers are arranged in

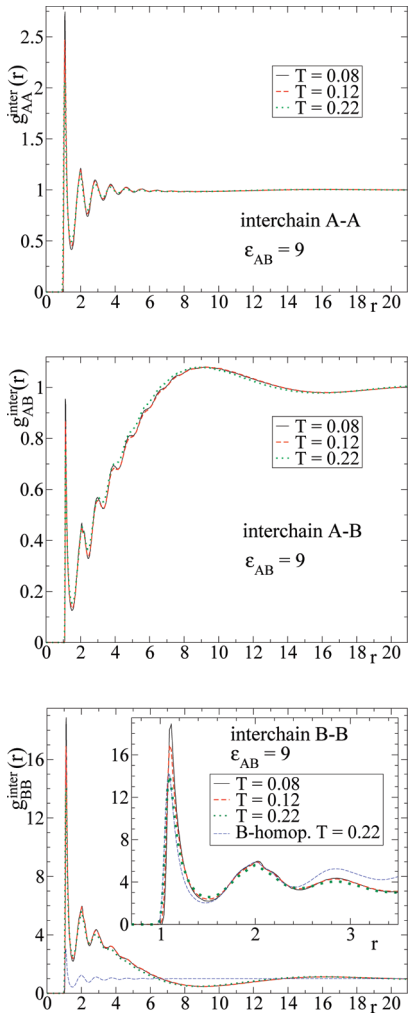

Figure 3. For $\epsilon_{AB}=9$, T-dependence of radial distribution functions for interchain correlations (top, A−A; middle, A−B; bottom, B−B). The bottom panel also shows the corresponding results for the B-homopolymer at $T = 0.22$. The inset displays the same data sets at short distances, though now data for the B-homopolymer are rescaled for comparison with the diblock system at $T = 0.22$ (see text).

disconnected domains, leading to a spherical micellar phase. On passing, we note that short-ranged B−B interchain correlations in the micellar cores are, as in the homogeneous phase, rather similar to those of the B-homopolymer at the same T (see inset in the bottom panel).

The arrangement of the diblock chains in a spherical micellar phase for $\epsilon_{AB} = 9$ is confirmed by representing snapshots of the micellar cores. We define a micellar core as the set of B-monomers belonging to a same cluster of chains. The used criterium for clustering is that two distinct chains i and j belong to a same cluster if there is at least one B-monomer of i at a distance $r < r_{min}$ from at least one B-monomer of j. For the case $\epsilon_{AB} = 9$, we take the value $r_{min} = 1.5$, which corresponds to the first minimum in the interchain radial distribution function $g_{BB}^{inter}(r)$ represented in Figure 3. In Figure 4, we show a typical snapshot of all the micellar cores in the simulation cell for $\epsilon_{AB} = 9$ and $T = 0.08$. For clarity, we just represent the positions of the centers-of-mass of the B-blocks. The cores are not arranged in an ordered structure. Since the expected equilibrium structure is a bcc lattice, the obtained phase is, in principle, metastable (see below). The *spontaneous* formation of a *crystalline* lattice of spherical micelles in simulation time windows is difficult even for semiconcentrate solutions[49], and would involve prohibitive time scales for melt densities as in the present case. Having said this, we believe that

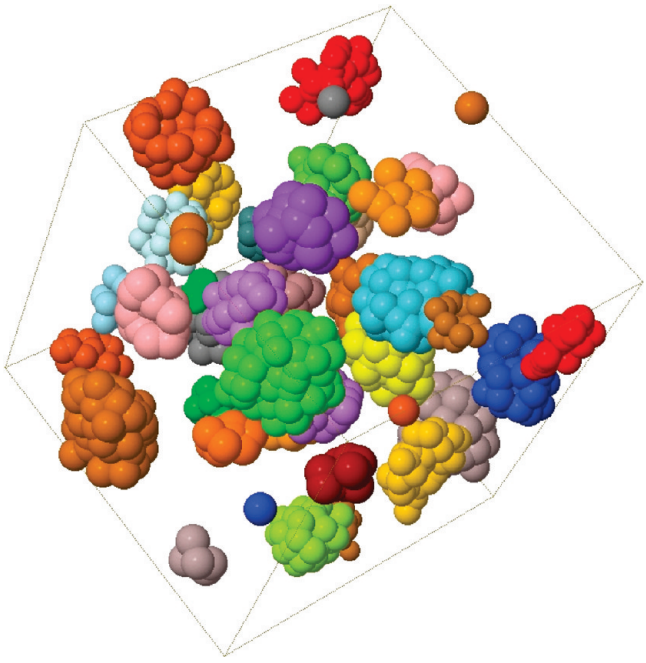

Figure 4. Typical snapshot of the simulation cell for $\epsilon_{AB} = 9$ and $T = 0.08$. Note the periodic boundary conditions. The cell axes are represented for clarity. The spheres represent the positions of the centers-of-mass of the B-blocks. Different micellar cores are represented with different colors.

the presence or absence of long-range order does not have major effects on the local dynamics of the B-monomers in the cores, which are in principle dominated by short-range confinement effects induced by the interface and by fluctuations of the latter. Thus, we believe that the qualitative dynamic picture presented in this work is also valid for the ordered bcc phase.

In order to demonstrate the metastability of the obtained micellar phase, we compute the distinct part of the van Hove correlation function for monomers located at different chains. Figure 5 displays results for A−B and B−B interchain correlations at fixed $\epsilon_{AB} = 9$ and $T = 0.22$, for several times from $t = 0$ to the limit of the simulation window. As usually observed in glass-forming liquids, structural relaxation leads to the decay of static correlations at short length scales. However no signature of relaxation occurs for correlations observed at larger scales $r \gtrsim 5$, which probe the microsegregated domains. Similar results (not shown) are obtained for $\epsilon_{AB} = 9$ at the other investigated temperatures, and also at all temperatures for the case $\epsilon_{AB} = 2$. From these observations, we conclude that the spherical micellar phase is metastable at least within the simulation time scale.

A total of 27 micelles are identified in the simulation cell according to the criterium introduced above, with an average aggregation number of $\langle n_{agg} \rangle = 38.9$ chains per micelle. The aggregation number is strongly polydisperse (see also below), with a large standard deviation, $(\langle n_{agg}^2 \rangle - \langle n_{agg} \rangle^2)^{1/2} = 22.5$. This strong polydispersity in the spontaneously formed phase is not, in principle, expected for the equilibrium crystalline phase. Having noted this, we will demonstrate in section IV that polydispersity in the micellar size is just a minor source of dynamic heterogeneity for relaxation of the B-blocks.

The micelles do not change their identity during the production runs. More specifically, no micellar fusion/fision or chain exchange is observed, and the set of chains associated with a given micelle (i.e., belonging to a same cluster as explained above) is unchanged. Thus, chain diffusion is suppressed in the time scale of the simulation and the B-monomers are effectively confined within the micellar cores.

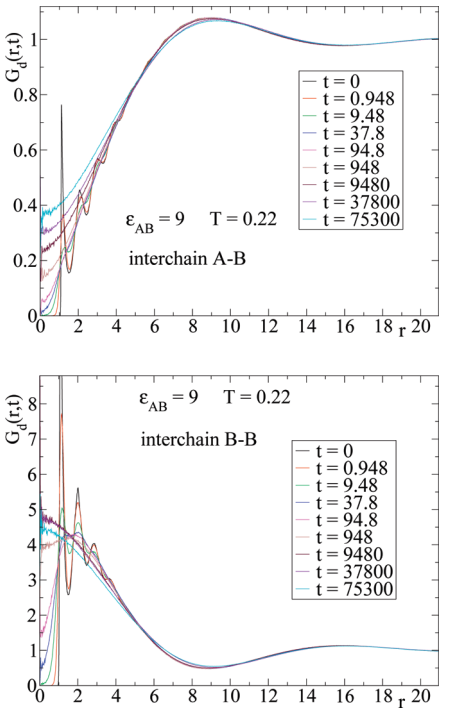

Figure 5. For $\epsilon_{AB} = 9$ and $T = 0.22$, time dependence of the van Hove distinct functions for interchain correlations of A−B (top) and B−B (bottom) pairs.

In order to obtain a qualitative characterization of the size and shape of each micellar core, we compute the inertia axes of the set of B-monomers directly linked to the A-blocks of the chains constituting the micelle. Figure 6 shows the results of this analysis for $\epsilon_{AB} = 9$ and $T = 0.22$. In panel a, we represent the major (D_{max}), middle (D_{mid}), and minor (D_{min}) axes of the 27 micellar cores in the system. Micelles are labeled by increasing order of the major axis and identical labels in the other panels of Figure 6 correspond to the same micelle. The numerical values represented in panel a are averages over 20 different configurations at equispaced times. Panel b shows the corresponding standard deviations. The ratios D_{max}/D_{min} and D_{mid}/D_{min} are represented in panel c. Finally, panel d shows the aggregation number of each micelle. As mentioned above, the latter is strongly polydisperse, with values from 3 to 89 chains. As expected, the size of the inertia axes, typically between 6 and 8 for D_{max}, exhibits a clear correlation with the aggregation number. However, no correlation is apparently observed for the standard deviation of the inertia axes. Panel c shows that the shape of the micellar cores is close to the ideal spherical case. Thus, typical values of the ratio of the major over the minor axis are smaller than 1.2. Results at lower temperatures for the quantities displayed in panels a−d show similar values.

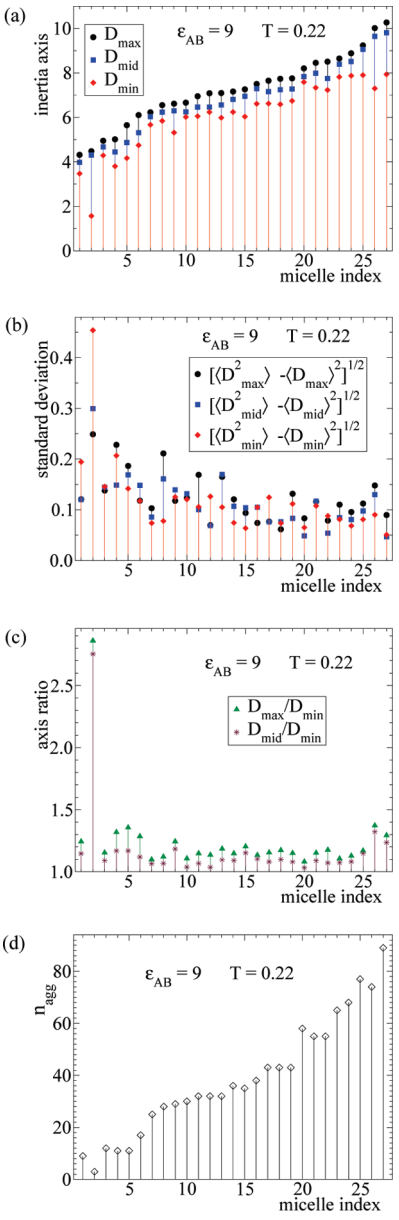

Figure 6. For $\epsilon_{AB} = 9$ and $T = 0.22$, characterization of the size of all the micellar cores in the simulation cell. Abscisas are labels for identifying the different micelles. We assign the same label to each micelle in the four panels. Vertical lines are guides for the eyes. For each micelle, data in panels a−c correspond to averages over 20 configurations at equispaced times. Panel a: major, middle, and minor inertia axes (see text for definition). Note that labels are assigned by increasing order of the major axis. Panel b: standard deviation for the inertia axes. Panel c: ratios of major and middle axes over the minor axis. Panel d: micellar aggregation number.

IV. Dynamic Features

A. Orientational Dynamics. In this section we characterize the relaxation of several dynamic correlators probing the dynamics within the micellar cores, as well as the mobility of the interface. Figure 7 displays results for the orientationl correlator of the end-to-end vector of A- and B-blocks. The latter is defined as the Legendre polynomium of first order $P_1(\theta_{ee}(t)) = \langle \cos\theta_{ee}(t)\rangle$, where $\theta_{ee}(t)$ is the angle formed between the end-to-end vector at $t = 0$ and the same at the considered time t. The average is done over all the considered blocks. Data in Figure 7 correspond to all the investigated values of T and ϵ_{AB}. Results for the corresponding homopolymers at the same temperatures are also displayed for comparison. The reorientation of the end-to-end vector of the A-block is clearly slowed down in comparison to the A-homopolymer at the same temperature. This effect becomes stronger by decreasing temperature and by increasing the ϵ_{AB} parameter.

In agreement with the experiments by dielectric spectroscopy on PI/PDMS cited in the Introduction[46], the end-to-end reorientation of the B-block is accelerated, in comparison to the B-homopolymer at the same temperature, at short and intermediate times for all the investigated cases. This effect is spectacular for low temperatures $T = 0.08$ and $T = 0.12$. Thus, the temperature dependence of the initial reorientation is much weaker for the B-block than for the B-homopolymer.

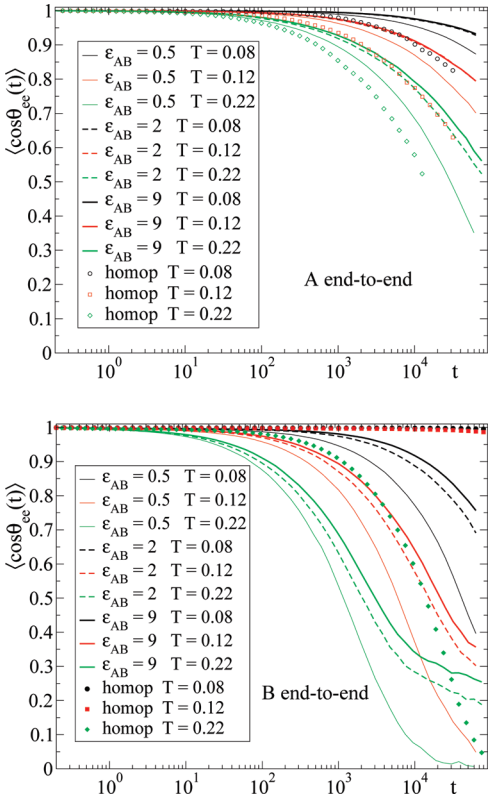

Figure 7. Top panel: Orientational correlator of the end-to-end vector of the A- (top) and B-blocks (bottom). Data for the corresponding homopolymers are included for comparison. Temperatures and ϵ_{AB} parameters are given in the legend.

The reorientation of the B-blocks at long times for the highest investigated temperature $T = 0.22$ shows two rather distinct features for the homogeneous and micellar phases. While in the homogeneous phase ($\epsilon_{AB} = 0.5$) the separation between the time scales of the B-block and the B-homopolymer is maintained until full relaxation is reached, in the micellar phase an apparent plateau arises for reorientation at long times. This plateau is higher for stronger cross-interaction energy ϵ_{AB}.

From these observations a temptative physical picture arises for the reorientation of both blocks. The coupling to a block of very different intrinsic mobility strongly changes the initial time scale for reorientation, which is slowed down or accelerated in comparison to the homopolymer state at the same temperature. This effect is particularly strong for the B-blocks, which are strongly coupled to the dynamics of the majoritary (note that $f_A = 0.87$) and intrinsically much faster A-component. On the contrary, the effect is moderate for the A-blocks, which are less affected by the presence of the minority B-component ($f_B = 0.13$). Even if the time scale is accelerated for the B-blocks, the presence of the interface in the micellar phase frustrates full reorientation within the time scale of the simulation, yielding a plateau in the correlator. We expect that a plateau is present for both components in the micellar phase at all temperatures, though due to the limited time window of the simulation it is only observed for the B-block at $T = 0.22$.

Similar trends are observed for the case of the reorientation of bond vectors between consecutive monomers of a same block. Figure 8 shows the corresponding correlators $P_1(\theta_b(t)) = \langle \cos\theta_b(t) \rangle$. The latter are averaged over all the bonds of type A−A or B−B. Reorientation of A−B bonds will be discussed below. On passing, comparison of data for

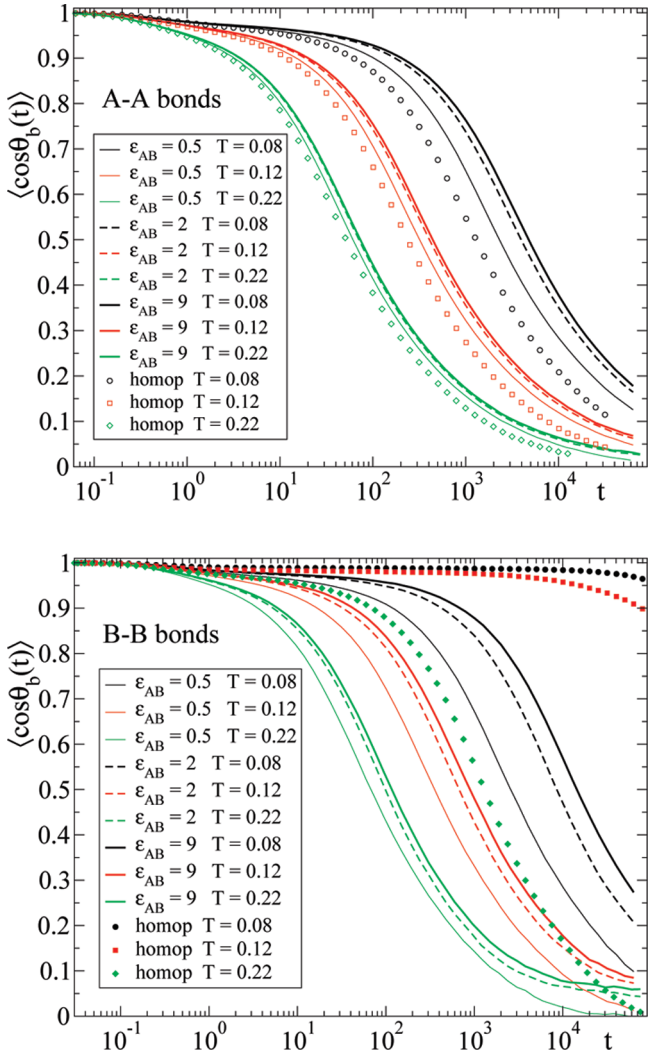

Figure 8. Orientational correlator for bonds between consecutive monomers, both for the blocks and the corresponding homopolymers. Top and bottom panels show data for respectively A−A and B−B bonds. Temperatures and ϵ_{AB} parameters are given in the legend.

the two homopolymers reveals a strong separation of their time scales at the same temperature, with a much faster dynamics in the A-homopolymer. In this way we confirm the conditions that were aimed by the selected values of ϵ_{AA} and ϵ_{BB} (see above). A long-time plateau is again observed for the micellar phase. The amplitude of the plateau is smaller than in the case of the end-to-end vector. Since bond reorientation involves a much smaller length scale than reorientation of the end-to-end vectors, one might suggest that the former is less affected by the presence of the interface, therefore leading to a smaller plateau. However we show now that this idea must be taken with care. Since presumably the presence of the interface has a much weaker effect for bonds close to the block ends than for bonds close to the interface (and in particular for A−B bonds) the features presented in Figure 8 can arise as the average of a relaxation map which is strongly dependent on the bond location. This is indeed confirmed by computing orientational correlators of single bonds. Thus, by using the label i for the bond connecting the monomers i and $i + 1$, we compute the former correlators by averaging over all the i-bonds of the different chains in the system. We enumerate the bonds by starting from the A-end. In this way, $i = 1$ and $i = 69$ correspond respectively to the terminal A−A and B−B bonds. The A−B bond is denoted as $i = 61$. Figure 9

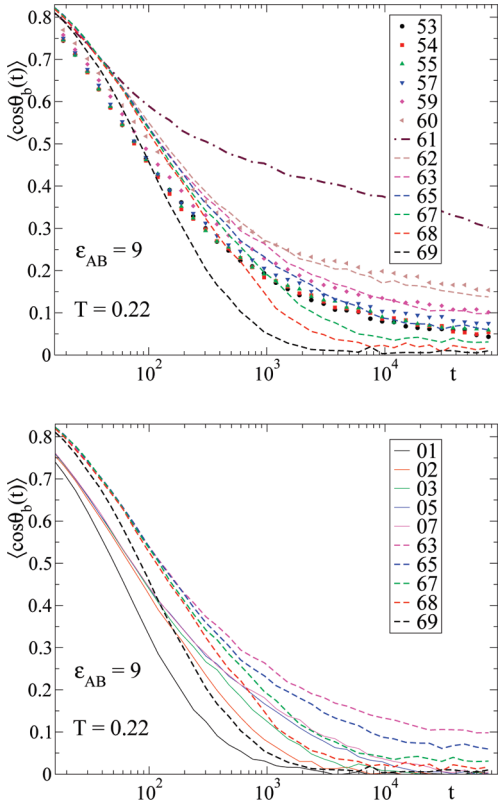

Figure 9. For $\epsilon_{AB}=9$ and $T=0.22$, orientational correlator for selected bonds between consecutive monomers. Labels i in the legend denote bonds between monomers i and $i+1$. Data for bond counterparts (see text for definition) are represented in separate panels for clarity.

shows, for $\epsilon_{AB}=9$ and $T=0.22$, results for several selected bonds. The data reveal that reorientation is strongly dependent on the location of the considered bond along the chain. As can be seen in Figure 9, reorientation of the A−B bond in particular, and of bonds close to it in general, is extremely slow in comparison to reorientation of bonds close to the chain ends. Only for the latter full relaxation is observed within the time scale of the simulation. This is true even for the bonds close to the end of the B-block, which are confined within the micellar cores. Such bonds are not, on average, close to the interface, and the latter does not hinder their reorientation. Note that just a very weak plateau is observed for the bond $i=68$. For $i=69$ no plateau can be resolved within statistics.

In the top panel of Figure 9 we show correlators $P_1(\theta_b(t))$ for B−B bonds $i=61+j$ (with $1\le j\le 8$) and the corresponding "counterpart" A−A bonds which are located at symmetric positions starting from the A−B bond (i.e., $i=61-j$). Note that data for A−A and B−B bonds are represented respectively by symbols and lines, and with identical colors if they are counterparts according to the former definition. At short time scales the reorientation of a given B−B bond is systematically slower than the reorientation of its A−A counterpart at the other side of the interface. This can be understood as a consequence of the higher mobility of the A-monomers in that time scale, which still does not probe the coupling between A- and B-blocks. At longer time scales, and specially when the interfacial effects are probed, the opposite trend is observed. Thus, the correlators of counterpart bonds cross each other and the reorientation of a B−B bond becomes systematically faster than the reorientation of its A−A counterpart. The separation of the time scales of counterpart bonds becomes stronger if the B−B bond is closer to the end of the

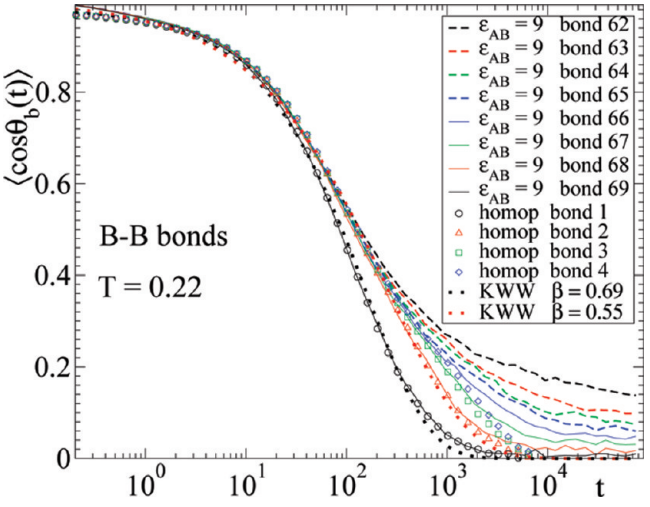

Figure 10. For the micellar phase with $\epsilon_{AB}=9$ (dashed and solid lines) and for the B-homopolymer (empty symbols), orientational correlator for selected B−B bonds at $T=0.22$. Labels i in the legend denote bonds between monomers i and $i+1$. The time scale of the B-homopolymer is divided by 11.7 to obtain superposition with data of the B-block. The dotted lines are fits to KWW functions. The stretching exponents are given in the legend.

B-block. Thus, at long time scales the influence of the intrinsic mobility (which is higher for the A-monomers) is less relevant than the distance to the chain end. The terminal B-bonds have more freedom to rotate than inner A-bonds, and despite of their lower intrinsic mobility in comparison to the A-bonds, they exhibit a faster reorientation.

The bottom panel of Figure 9 also compares orientational correlators for B−B bonds i (dashed lines) and A−A counterparts (solid lines with common colors), but now the latter are defined as the bonds $i'=70-i$. Hence we compare the reorientation of a B−B bond at a given distance from the B-block end, and that of an A−A bond located at the same distance from the A-block end. Since the selected A−A bonds are far from the interface, the latter does not influence their reorientation and no plateau arises at long times. Thus, as a consequence of its higher intrinsic mobility, they exhibit at all times a faster reorientation than their B−B counterparts.

It is also interesting to compare the degree of dynamic heterogeneity for bond reorientation in the micellar phase and in the corresponding homopolymer state. By doing this, new dynamic features are revealed. Figure 10 displays data, at $T=0.22$, for $P_1(\theta_b(t))$ of selected B−B bonds, both in the micellar phase with $\epsilon_{AB}=9$ and in the B-homopolymer. Bonds in the homopolymer are labeled as $i=1,2,\ldots,8$ from one to the other chain end. Since as expected, results for the bonds i and $9-i$ in the B-homopolymer are, by symmetry, identical within statistics, only data for $i\le 4$ are represented. A much weaker dynamic heterogeneity for bond reorientation is observed for the homopolymer in comparison to the results in the micellar phase. For a more detailed comparison with data for the B-block, we define now the counterparts of a selected bond $i\le 4$ of the B-homopolymer as those in the B-block at the same position starting from the block ends. More specifically the latter are the bonds $i'=70-i$ and $i'=61+i$, which we respectively denote as the "outer" and "inner" counterparts. Note that data for counterpart bonds are represented with identical colors in Figure 10 (empty symbols for bonds in the B-homopolymer, solid and dashed lines for respectively the outer and inner counterparts in the B-block). Comparison of results for counterpart bonds reveal a nontrivial time scaling. Data for all the selected

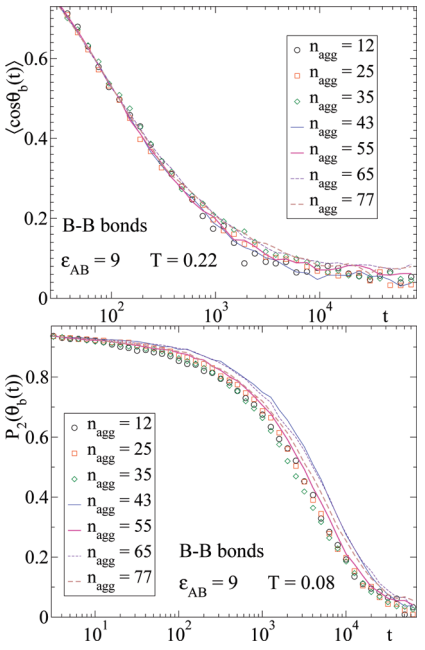

Figure 11. For $\epsilon_{AB} = 9$, orientational correlators (see text) for B−B bonds at $T=0.22$ (top) and $T=0.08$ (bottom). Each data set corresponds to a different selected micelle. The corresponding aggregation numbers are given in the legend.

bonds of the B-homopolymer have been divided by a common factor 11.7 in order to demonstrate superposition with data for the B-block. The scaling behavior is fulfilled at intermediate times for each bond in the B-homopolymer and its two counterparts in the B-block, and breaks when the plateau regime associated with the interface (which is absent for the homopolymer) is probed at longer times. The fact that the decay prior to the plateau regime is strongly nonexponential suggests a nontrivial origin for the observed scaling. Nonexponentiality is demonstrated by fitting the former decay to an stretched exponential or Kohlraush−Williams−Watts (KWW) function, $\propto \exp[-(t/\tau)^{\beta}]$. Hence, we obtain an exponent $\beta = 0.69$ for the end bonds $i = 1$ and $i' = 69$, and $\beta = 0.55$ for $i = 2$ and $i' = 68$.

In Figure 9, we have demonstrated that the specific location along the chain is a source of strong dynamic heterogeneity for bond reorientation at long times. Thus, time scales for reorientation can exhibit extreme differences between bonds close the interface and those close to the chain ends. It might be expected that the observed polydispersity in the micellar aggregation number (see above) is also an additional source of dynamic heterogeneity. Now we show that the latter has actually a small effect in comparison to the specific location of the bond along the chain. The top panel of Figure 11 shows results, for $\epsilon_{AB}=9$ and $T=0.22$, for orientational correlators $P_1(\theta_b(t))$ of B−B bonds of several selected micelles. Thus, each correlator is computed by averaging over all the B−B bonds belonging to a same micellar core. The aggregation numbers of the selected micelles are given in the legend and cover esentially all the range of observed values (see Figure 6). Within statistical uncertainties, the decay of the correlators shows a rough dependence on the micellar size, being slower for larger aggregation. However, the dispersion in the data sets is very weak, in comparison to that observed in Figure 9 for reorientation of specific bonds at the same temperature and cross-interaction energy ϵ_{AB}. Analogous results for A−A bonds (not shown) also exhibit a very weak dependence on the micellar size.

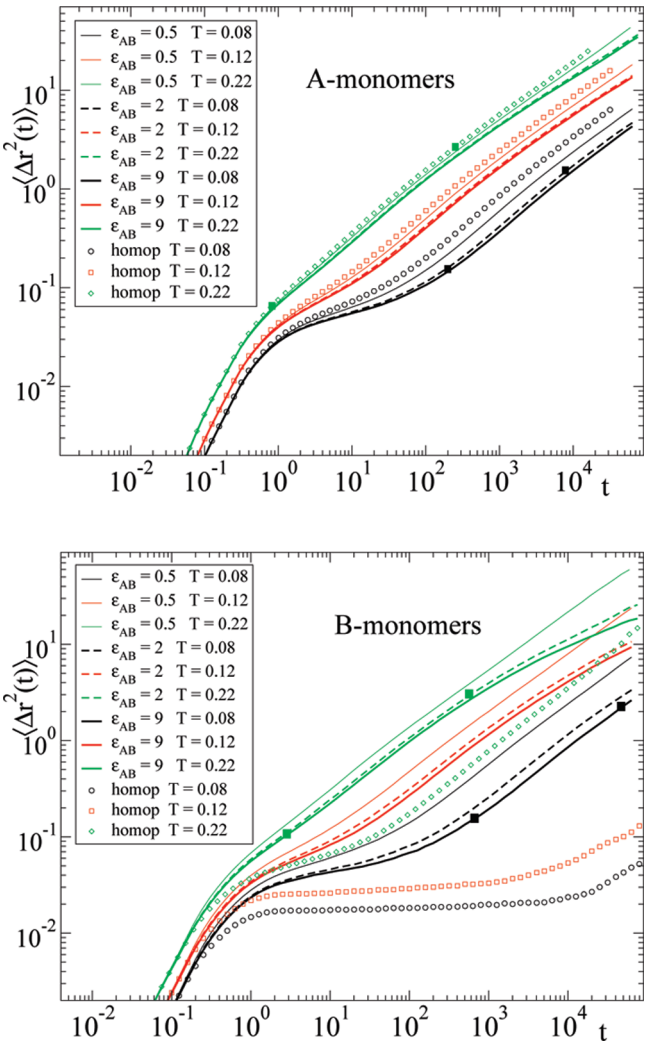

Figure 12. Mean squared displacement. Top and bottom panels show results for respectively A- and B-monomers. Data for the diblock systems are represented with lines. Temperatures and ϵ_{AB} parameters are given in the legend. Data for the homopolymers (symbols) at the same temperatures are included for comparison. Filled squares delimit representative regions of approximate subdifussive behavior $\langle \Delta r^2 \rangle \sim t^{0.6}$.

Even by decreasing temperature (which enhance dynamic heterogeneity of local reorientations in glass-forming polymers[50,51]) we still observe a moderate dispersion in the orientational correlators of selected micelles. This is demonstrated in the bottom panel of Figure 11, which shows results, for $\epsilon_{AB} = 9$ and $T = 0.08$, for the orientational correlator $P_2(\theta_b(t))$ for the B−B bonds. The latter corresponds to the Legendre polynomium of second order. We represent this correlator since it shows an almost full relaxation at this temperature. Having said this, the corresponding data for $P_1(\theta_b(t))$ (not shown) exhibit, within the simulation time window, a similar dispersion.

Finally, we have computed analogous orientational correlators for block end-to-end vectors of selected micelles (not shown). We observe a similar moderate dispersion even at low temperature.

B. Translational Dynamics. A similar analysis to that above presented for orientational relaxation can be performed for the translational dynamics. Figure 12 displays results for the mean squared displacement, $\langle \Delta r^2(t) \rangle$, of A- and B-monomers for all the investigated values of T and ϵ_{AB} in the diblock system. The corresponding data

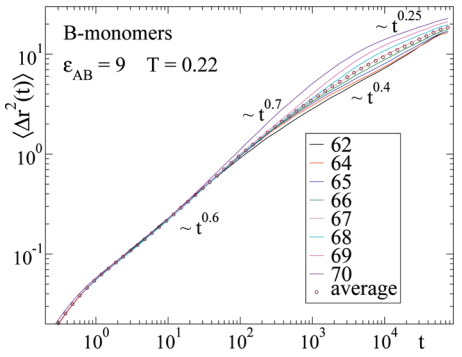

Figure 13. For $\epsilon_{AB} = 9$, mean squared displacement for selected B-monomers at $T = 0.22$. The average over all B-monomers is included for comparison. The indicated power-law regimes are rough approximations. They are just shown for quantifying deviations from diffusive linear behavior.

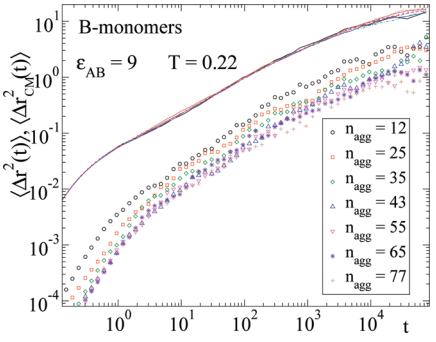

Figure 14. For $\epsilon_{AB} = 9$ at $T = 0.22$, mean squared displacement for B-monomers (lines) and for centers-of-mass of micellar cores (symbols). Each data set corresponds to a different selected micelle. The corresponding aggregation numbers are given in the legend. Data for a same micelle are represented with identical colors.

for the homopolymers at the same temperatures are included for comparison. At this point, data are averaged over all the A- and B-monomers in the system (results for selected monomers will be discussed below). Comparison between data of the two homopolymers show again a strong separation of the time scales at a same temperature, with a much faster dynamics for the A-homopolymer. Mean squared displacements in the diblock exhibit trends similar to those observed for the orientational dynamics. Thus, the translational motion of the A- and B-monomers is respectively slowed down and accelerated in comparison to results in the homopolymer at the same temperature. This effect is again impressive for the dynamics of the B-monomers, specially at low temperatures, and moderate for the A-monomers.

After the initial ballistic regime $\langle \Delta r^2 \rangle \sim t^2$ for $t \lesssim 0.3$, a bending is observed in the mean squared displacement, which becomes a plateau for low temperatures. The latter is associated with the well-known caging regime characteristic of glass-forming liquids, which originates from the temporary mutual blocking between neighboring particles. At longer times, the cage is broken and structural relaxation takes place, leading to an ultimate linear diffusive regime $\langle \Delta r^2 \rangle \sim t$ for simple fluids. This is not the case of polymer systems, which usually exhibit several subdiffusive regimes, $\langle \Delta r^2 \rangle \sim t^z$ with $z < 1$, prior to the final crossover to linear behavior at much longer times. The observed power-law (see Figure 12) with $z \approx 0.6$ is close to the prediction of the ideal Rouse model[52,53], $z = {}^1/_2$.

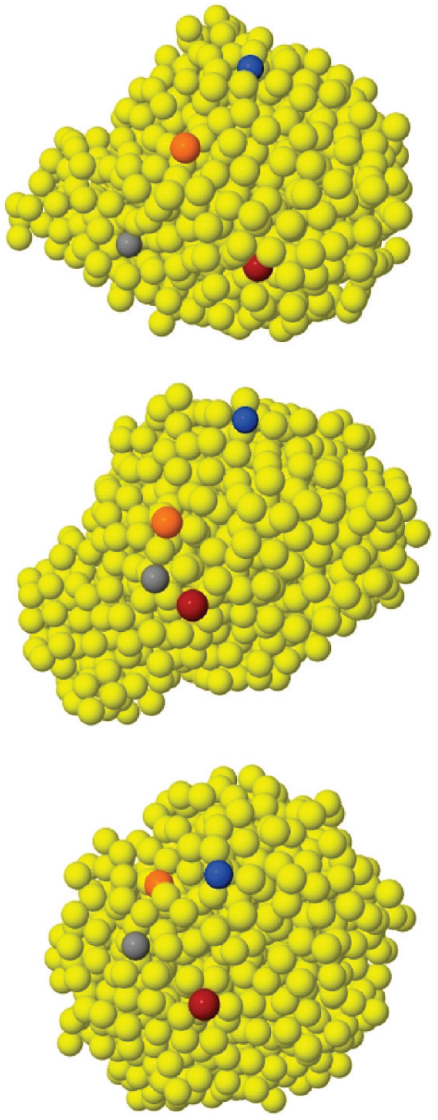

Figure 15. For $\epsilon_{AB} = 9$ and $T = 0.12$, snapshots of the B-monomers of a selected micelle ($n_{agg} = 55$) at different times, $t = 0$, 3×10^4, and 6×10^4 (from top to bottom). In order to visualize characteristic interfacial fluctuations, a few monomers are represented in different colors.

For strongly entangled chains ideal reptation theory[52,53] predicts a crossover from Rouse behavior to a second sublinear regime with $z = {}^1/_4$. This ideal regime is approached only for chains much longer than those of the present model. For shorter entangled chains subdiffusive behavior with an effective exponent ${}^1/_4 < z < {}^1/_2$ typically arises after the Rouse-like regime[47,54,55]. This is the case for the A-homopolymer chains ($z \sim 0.45$, not indicated), which are weakly entangled—the entanglement length for similar bead−spring homopolymers is $N_e \approx 35$ monomers[47]. Entanglement effects are difficult to quantify in the micellar phase, since for the time scales in which they are expected, monomer displacements start to probe interfacial effects. Thus, for values $\langle \Delta r^2 \rangle \approx 3$, data for the micellar phases ($\epsilon_{AB} = 2$ and 9) exhibit a bending, presumably toward a long-time plateau regime. The latter would originate, as that observed for the orientational dynamics, from confinement effects associated with the interface. The role of the interface on entanglements, and namely the effect on the diffusivity, has been discussed in some studies of lamellar phases.[19,22,28,29] Interfacial effects on entanglements in the present micellar phases and its role,

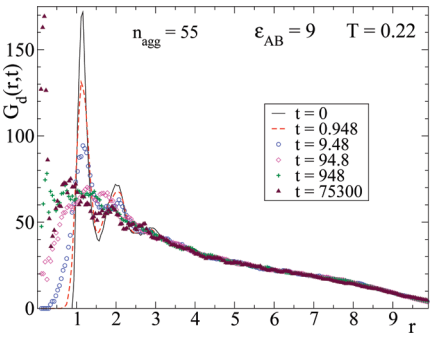

Figure 16. For $\epsilon_{AB} = 9$ at $T = 0.22$, time dependence of the van Hove distinct-correlation function for the B-monomers directly linked to the A-blocks of a selected micelle (with $n_{agg} = 55$).

if any, on the observed bending are beyond the scope of this work and are not discussed here.

We investigate now the translational dynamic heterogeneity associated with the specific location of the monomers. Figure 13 shows results for the mean squared displacement of B-monomers in the micellar phase with $\epsilon_{AB} = 9$, at $T = 0.22$. Data are given both for the average over all the B-monomers in the system and over B-monomers in specific locations. In analogy with the bond labeling (see above), $i = 62$ denotes the B-monomer connected to the A-block and $i = 70$ the terminal B-monomer. A bifurcation of the data for the different monomers is observed at $\langle \Delta r^2 \rangle \sim 0.3$, while for long times the data tend to collapse again. At intermediate times, mean squared displacements are larger for terminal monomers. For the latter, deviations above the average grow up significantly until displacements start to probe the interfacial effects. At this point, the end monomers experience a strong slowing down (note the rough power-law $\langle \Delta r^2 \rangle \sim t^{0.25}$) and convergence to a common curve for all the monomers is approached.

As previously done for the orientational dynamics, we also investigate the effect of the polydispersity of the micellar cores in the translational dynamic heterogeneity. Figure 14 shows, for $\epsilon_{AB} = 9$, results for the mean-squared displacement of the B-monomers at $T = 0.22$. Each data set corresponds to a different micelle, and is computed by averaging over all the B-monomers of the respective micellar core. We have selected the same representative micelles as in the case of the orientational dynamics (see Figure 11). As observed for bond reorientations, polydispersity of the micellar cores has a very weak effect, at least in the simulation time window, on the translational dynamic heterogeneity.

In the same figure, we also represent the mean-squared displacement for the centers-of-mass of the same selected micellar cores. Data for the smallest and largest one differ just by a factor of $\lesssim 4$. As expected for an oscillatory motion of the micellar centers, a plateau seems to arise at long times. The amplitude of such oscillations are of about 1−2 monomer diameters.

C. Interfacial Mobility. To finish this section, we show that the micellar interface exhibits a strong internal mobility. Figure 15 shows snapshots of the B-monomers of a representative selected micelle ($n_{agg} = 55$) at different times $t = 0$, 3×10^4, and 6×10^4. The three frames are represented in the reference system of the center-of-mass of the micellar core. The coordinate axes (not shown) are fixed and equally oriented in the three frames. The motion of a few B-monomers directly linked to the A-blocks is visualized by representing them with different colors. Strong fluctuations for the monomer positions as well as for their relative distances are clearly observed.

A more detailed characterization of the interface mobility is obtained by computing the van Hove distinct function for the all the B-monomers directly linked to the A-blocks of the selected micelle. Figure 16 shows the so-obtained results. A clear relaxation of the short-ranged static correlations is observed as a consequence of the internal motion of the interface.

V. Discussion: Analysis of Rouse Modes

In the previous Sections we have presented a huge set of results for the spherical micellar phase of an AB-diblock copolymer for which the corresponding A- and B-homopolymers exhibit very different mobilities. Specifically, the B-homopolymer, which forms the cores in the micellar phase, has a much higher glass transition temperature than the A-homopolymer. We have provided evidence for a strong coupling of the dynamics of the B-blocks to that of the A-blocks in the micellar phase. This leads to a dramatic acceleration of the intermediate time scale of the B-component, as well as to a high internal mobility of the micellar interface.

These features may suggest that the dynamic coupling to the A-blocks has a certain degree of stochastic character, perhaps contributing through an effective friction. A strictly stochastic coupling of a tagged chain to its surroundings, with an effective friction, is the main assumption of the Rouse model (see below), which provides a simple physical picture for the dynamics of nonentangled polymer melts. Computational tests for simplified bead−spring homopolymers as those investigated here confirm the main qualitative predictions of the Rouse model. In this Section we analyze the limits of validity of the Rouse model for the dynamics of the B-blocks in the micellar phase.

Now we summarize the main predictions of the Rouse model[52,53]. A tagged chain is represented as a string of N beads (monomers) of equal mass connected by harmonic springs of constant $3k_BT/b^2$, with b the bond length. The effective interaction experienced by the chain is given by a friction coefficient ζ and a set of stochastic forces $\mathbf{f}_j$. Excluded volume interactions are neglected. The corresponding equations of motion for each monomer of the tagged chain are solved by introducing normal modes (Rouse modes), of index $p = 1, ..., N-1$, which are defined as follows:

$$\mathbf{X}_p(t) = N^{-1} \sum_{j=1}^{N} \mathbf{r}_j(t) \cos[(j-1/2)p\pi/N] \tag{3}$$

The Rouse modes follow the equations of motion

$$2N\zeta \dot{\mathbf{X}}_p = -k_p \mathbf{X}_p + \mathrm{g}_p \tag{4}$$

with $k_p = 24Nk_BTb^{-2} \sin^2[p\pi/2N]$. The quantity $\mathbf{g}_p$ is the external force for the pth-mode and is given by $\mathbf{g}_p(t) = 2\Sigma_{j=1}^{N} \mathbf{f}_j(t) \cos[jp\pi/N]$. Integration of the equations of motion yields

$$\langle \mathbf{X}_p(t) \cdot \mathbf{X}_q(0) \rangle = (2N\zeta)^{-2} \int_{-\infty}^{t} \mathrm{d}t' \, \mathrm{e}^{-(t-t')/\tau_p} \times \int_{-\infty}^{0} \mathrm{d}t'' \, \mathrm{e}^{t''/\tau_q} \langle \mathbf{g}_p(t') \mathbf{g}_q(t'') \rangle \tag{5}$$

for the correlators of the Rouse modes. The relaxation time of the pth-mode is given by

$$\tau_p = (b^2\zeta/12k_BT) \sin^{-2}[p\pi/2N] \tag{6}$$

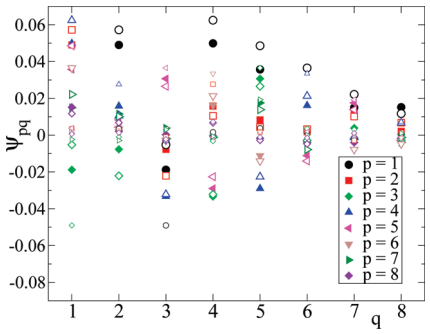

Figure 17. Orthogonality test for the Rouse modes of the B-block. Big filled and big empty symbols correspond to ψ_{pq}-values (see text) for the diblock systems ($\epsilon_{AB} = 9$) at respectively $T = 0.08$ and $T = 0.22$. Small empty symbols correspond to the B-homopolymer at $T = 0.22$. Same color and symbol type corresponds to same values of (p,q).

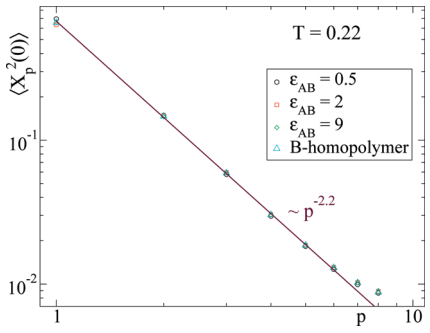

Figure 18. At $T = 0.22$, comparison between the amplitudes $\langle X_p^2(0)\rangle$ of the Rouse modes for the B-block (for several values of ϵ_{AB}) and for the B-homopolymer. The line is a power-law fit.

The Rouse model fully neglects spatial and time correlation of the stochastic forces. With this assumption the correlator of the forces becomes

$$\langle \mathbf{g}_p(t')\mathbf{g}_q(t'')\rangle = 12N\zeta k_B T\delta_{pq}\delta(t'-t'') \qquad (7)$$

The former two approximations yield respectively orthogonality and exponential relaxation of the Rouse correlators. Indeed, by introducing (7) in eq 5 we find

$$\langle \mathbf{X}_p(t)\cdot\mathbf{X}_q(0)\rangle = \left(\frac{b^2}{8N}\right)\sin^{-2}\left[\frac{p\pi}{2N}\right]\delta_{pq}e^{-t/\tau_p} \qquad (8)$$

Orthogonality and exponentiality of the Rouse modes are the two main predictions of the Rouse model, and are the basis for the derivation of correlators probing relaxation of chain degrees of freedom.[52,53]

We compute Rouse correlators for the B-blocks. This is done according to eq 3 with $N = 9$ by using only the coordinates of the B-monomers. In this way, the effects of the coupling of the tagged B-block to its corresponding A-block are effectively included, as for the rest of the surrounding chains, through the friction coefficient and the set of stochastic forces.

We first perform an orthogonality test for the so-defined Rouse modes for the B-blocks, by computing for all the pairs (p,q) the quantities $\psi_{pq} = \langle[\mathbf{X}_p(0)\cdot\mathbf{X}_q(0)]/[X_p(0)X_q(0)]\rangle$. These quantities are adequate for such a test since by construction $\psi_{pq} = \psi_{qp}$ and $\psi_{pp} = 1$. In Figure 17, we show results for $\epsilon_{AB} = 9$ at $T = 0.08$ and $T = 0.22$. Data for the B-homopolymer at $T = 0.22$ are also displayed for comparison. Since $\psi_{pp} = 1$ only the off-diagonal terms, $p \neq q$, are represented in an enhanced scale. We obtain small values $|\psi_{pq}| < 0.07$ for all the cases $p \neq q$ in the diblock system. The latter are only slightly larger than those for the B-homopolymer, $|\psi_{pq}| < 0.05$. Thus, we conclude that the Rouse modes as defined above for the B-blocks are still, concerning static correlations, good normal modes.

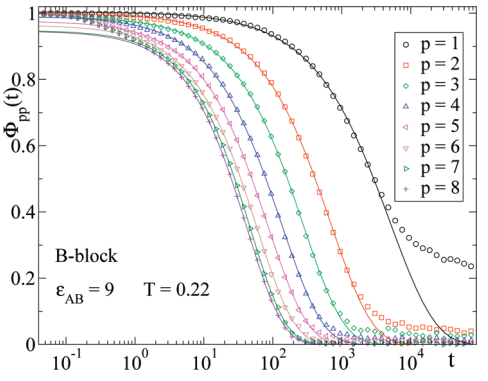

Figure 19. Rouse correlators of the B-blocks for $\epsilon_{AB} = 9$ at $T = 0.22$. Symbols are simulation data. Lines are fits to a KWW function.

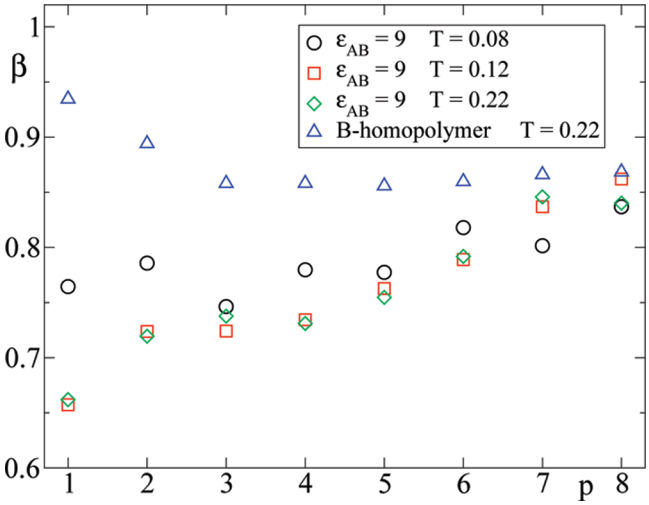

Figure 20. At several temperatures, stretching exponents from the KWW fits of Rouse correlators, for the B-homopolymer and the B-block ($\epsilon_{AB} = 9$).

Figure 18 shows, at $T = 0.22$, the p-dependence of the amplitudes of the Rouse modes, $\langle X_p^2(0)\rangle$, for all the values of ϵ_{AB}. Data for the B-homopolymer are also included for comparison. Within statistics, all data collapse in a master curve. This observation is also fulfilled at the other investigated temperatures (not shown), and is consistent with results shown above for the intrachain radial distribution functions (see Figure 1), which in the diblock systems are just weakly perturbed in comparison to the homopolymer state. Data follow an apparent power-law $\langle X_p^2(0)\rangle \sim p^{-2.2}$. The latter is consistent with previous results in similar bead−spring homopolymers[56,57] and indicate moderate deviations from ideal Gaussian behavior $\sim p^{-2}$ in the intrachain static correlations. Thus, from data in Figures 17 and 18, we conclude that eventual novel *dynamic* features for the Rouse modes of the B-blocks do not have their origin in their particular *static* features, which are esentially identical to those of the B-homopolymer.

Figure 19 shows normalized Rouse correlators $\Phi_{pp}(t) = \langle \mathbf{X}_p(t)\cdot\mathbf{X}_p(0)\rangle/\langle X_p^2(0)\rangle$ for the B-block with $\epsilon_{AB} = 9$ at $T = 0.22$. Data are shown for all the mode indexes p. Rouse modes of long wavelength (i.e., small p) exhibit a long-time plateau, which is absent both in the homopolymer state and in the homogeneous diblock (not shown here, see Figure 23 below). This plateau, which is in principle—as for the other correlators displayed in previous

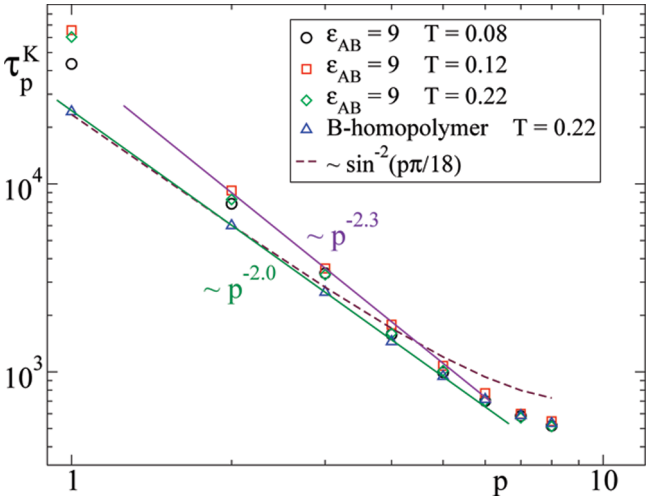

Figure 21. At several temperatures, KWW relaxation times for the B-homopolymer and the B-block ($\epsilon_{AB} = 9$). The solid lines are power-law fits. The dashed line indicates theoretical Rouse scaling for $N = 9$, i.e., $\sim \sin^{-2}(p\pi/18)$. Each data set has been multiplied by a common factor to obtain data overlap at large p. The factor for the B-homopolymer is 1. For the B-block the factors are 0.1, 1.7, and 11.7, for, respectively, $T = 0.08$, 0.12, and 0.22.

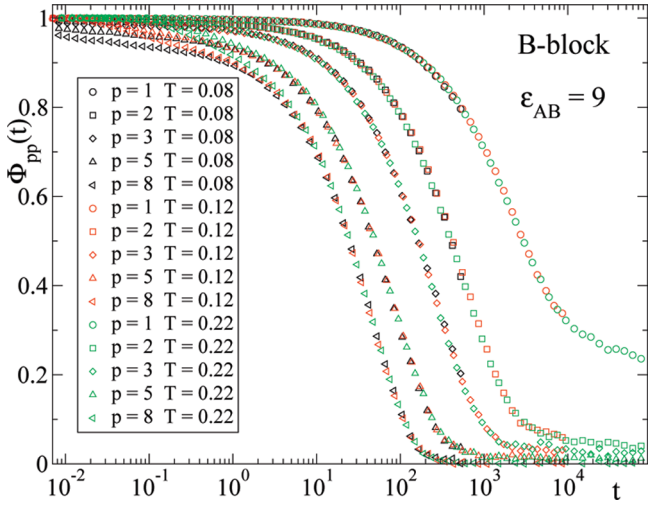

Figure 22. Rouse correlators of the B-block in the micellar phase ($\epsilon_{AB} = 9$), at several temperatures. The time scale of all the correlators at a same T is divided by a common factor, in order to yield data overlap with those at other T's. The factors are 1, 17, and 117 for respectively $T = 0.08$, 0.12, and 0.22.

sections—associated with the presence of the interface, is not provided by the standard Rouse model, which predicts a simple exponential decay (see eq 8). We suggested above that, due to the high intrinsic mobility of the A-monomers, the effect of the coupling to the A-block might be simply approximated as a contribution leading to an effective friction and stochastic forces acting on the tagged B-block, i.e., the ingredients of the Rouse model. However, the presence of the long-time plateau reveals a more complex physical mechanism.

In order to give account for the long-time plateau one might temptatively modify the Rouse model by connecting the tagged chain to an oscillating and/or fluctuating surface. Reorientational dynamics *at large scales* (e.g., of end-to-end vectors) for blocks attached to surfaces is not, in principle, independent of the geometry of the surface. Thus, we believe that the spherical shape of the interface should also be explicitly included in a modified Rouse model. The introduction and test of a model with the mentioned ingredients is beyond the scope of this work. Still, we can test to which extent, in time and length scales, the predictions of the Rouse model are consistent with our simulations.

First we quantify possible deviations of exponentiality before the onset of the long-time plateau. We fit data of the Rouse correlators to a KWW function, $\propto \exp[-t/\tau_p^K)^\beta]$. Appart from the long-time plateau, we also exclude from the fit the first decay up to $t \lesssim 3$. The latter corresponds to the microscopic monomer dynamics (see also mean squared displacements in section IV), which is implicitly coarse-grained in the Rouse model[52,53]. Illustrative fits for $\epsilon_{AB} = 9$ and $T = 0.22$ are shown in Figure 19. Figure 20 shows the p-dependence of the obtained stretching exponents β for $\epsilon_{AB} = 9$ at all the investigated temperatures. We also include the corresponding data for the B-homopolymer at $T = 0.22$. For $T = 0.08$ and $T = 0.12$ relaxation of the B-homopolymer is far beyond the simulation time window even for local scales (see also section IV) and fits cannot provide reliable parameters. Having said this, simulations of similar bead−spring homopolymers report just a very weak T-dependence of the β-exponents in the T-range for which relaxation is accessible[56]. As observed in previous works[56], Rouse correlators for the B-homopolymer are nearly exponential ($\beta \gtrsim 0.85$). The β-values in the micellar phase are systematically smaller than in the homopolymer, with stronger differences at small p.

Assuming than the standard Rouse model is still a good approximation at intermediate time and length scales in which relaxation is not still affected by the presence of the interface, one may interpret the observed stretched exponentials as the result of a distribution of intrinsically exponential processes. It is well-known that this is always possible at least formally, i.e., even if such processes are unphysical. From simple scaling arguments it can be seen[57] that if the mentioned distribution has a real physical origin, the obtained KWW times must obey the same scaling behavior predicted by the Rouse model, i.e., $\tau_p^K \propto \sin^{-2}(p\pi/N)$ (see above). Similarly, deviations from pure Rouse scaling will be a signature of intrinsic nonexponentiality. Figure 21 shows the p-dependence of the KWW times as obtained from the corresponding fits. As previously observed for similar models of nonentangled bead−spring homopolymers[56], data for the B-homopolymer follow approximate Rouse scaling, and hence stretching of Rouse correlators esentially arise from a distribution of elementary exponential process. The origin of such a distribution might be related to local structural heterogeneities leading to different local frictions. In principle, this effect is expected to play a more relevant role in the inhomogeneous micellar phase. Assuming that this is the case, it is not the only source for the observed nonexponentiality of the Rouse correlators of the B-blocks. For modes $p \geq 2$ deviations from intrinsic exponentiality are quantified through an effective power law $\propto p^{-2.3}$ (data for $p = 1$ are excluded since their KWW times are strongly affected by the presence of the plateau, see Figure 19). Still, these deviations are rather moderate in comparison with other physical situations as, e.g., power laws with anomalous exponents $\gtrsim 3$ for entangled homopolymers[58−60] or for the fast component in non-entangled blends with strong dynamic asymmetry.[57,61] Thus, the intrinsic exponentiality of the Rouse modes ($p \geq 2$) of the B-block can be viewed as a reasonable approximation.

Figure 22 shows Rouse correlators of the B-block, for $\epsilon_{AB} = 9$, at all the investigated temperatures. The time scales for all the mode indexes p at a common temperature have been divided by a common factor. Time−temperature scaling is demonstrated by the collapse of data from different temperatures. This apparently includes the plateau regime for the time window of the simulation, though the extent of the validity of the scaling cannot be determined. Since data in Figure 21 roughly show Rouse scaling, time−temperature superposition suggests a general scaling of the time scale as $\sim \zeta \sin^{-2}(p\pi/N)$, with a temperature-dependent

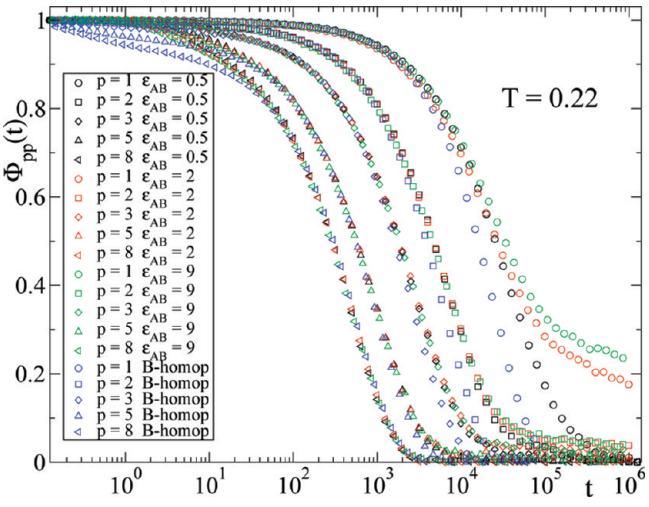

Figure 23. At $T = 0.22$, Rouse correlators of the B-homopolymer and the B-block (for several ϵ_{AB}-values). The time scale of all the correlators of a same system is divided by a common factor, in order to yield data overlap with those of other systems. The factor for the B-homopolymer is 1. For the B-block the factors are 0.048, 0.076, and 0.090 for respectively $\epsilon_{AB} = 0.5$, 2, and 9.

Table 1. For the B-Blocks, Estimated Ratio of Effective Frictions (See Text) $\zeta(\epsilon_{AB},T)/\zeta(\epsilon_{AB} = 9, T = 0.22)$

ϵ_{AB}	$T = 0.08$	$T = 0.12$	$T = 0.22$
0.5	19.5	2.6	0.53
2	71.7	5.4	0.84
9	117	6.9	1

effective friction ζ. This is the result which is expected from assuming the standard Rouse model (see eq 8).

Figure 23 displays Rouse correlators, for fixed temperature $T = 0.22$, both for the B-homopolymer and for the B-block at all the investigated values of ϵ_{AB}. The time scales of all the mode indexes p for a common ϵ_{AB} have been divided by a common factor. Again a collapse of all the data is observed for intermediate times. Interestingly, this time$-\epsilon_{AB}$ scaling is analogous to that previously observed for bond orientational correlators (see Figure 10). The scaling breaks at long times for low-order Rouse modes, for which the plateau is present in the micellar phases ($\epsilon_{AB} = 2$ and 9) and absent both in the homogeneous phase ($\epsilon_{AB} = 0.5$) and in the B-homopolymer. By using similar arguments as above suggested for intermediate scales not probing the interface (if existing), the effect of the coupling to the A-block is to introduce an ϵ_{AB}-dependent effective friction ζ for the tagged B-block. Since according to eq 6 $\tau_p \propto \zeta$, the time scaling of Figure 23 suggests that, at fixed $T = 0.22$, the effective friction for the B-block, $\zeta(\epsilon_{AB})$, is reduced in comparison to that of the B-homopolymer, ζ^{B}_{hom}, by the used factors for time scaling. Thus, we find $\zeta(\epsilon_{AB})/\zeta^{B}_{hom} = 0.048$, 0.076, and 0.090 for respectively $\epsilon_{AB} = 0.5$, 2, and 9. As mentioned above, relaxation times for the B-homopolymer are clearly beyond the simulation time window at $T = 0.08$ and $T = 0.12$ (see also Figures 8b and 12b), so the ratio $\zeta(\epsilon_{AB})/\zeta^{B}_{hom}$ cannot be estimated at these temperatures. Having said this, since Rouse mode times are accessible for the B-blocks for all the investigated values of ϵ_{AB} and T, it is clear that the former ratio at $T = 0.08$ and $T = 0.12$ is much smaller than at $T = 0.22$.

A global picture of the change of the effective friction with ϵ_{AB} and T in the diblock systems is provided by Table 1. The latter shows the ratio $\zeta(\epsilon_{AB},T)/\zeta(\epsilon_{AB} = 9, T = 0.22)$, which has been again estimated from time scaling factors. The lowest and highest obtained values for this ratio differ by a factor ≈ 220. This is a small variation in the effective friction in comparison to that observed for the B-homopolymer (which is far beyond the range accessible by the simulation, see above).

In summary, the results of this Section suggest that chain dynamics of the B-block is consistent, for intermediate time scales not probing the interface, with the Rouse model. In this framework, the effect of the coupling to the A-block enters through an effective friction which depends both on the temperature and the energy scale of the cross-interaction.

VI. Conclusions

We have reported a detailed characterization of the dynamic features of a simple model for melts of diblock (AB) copolymers. Molecular dynamics simulations of this model have been carried out at melt density, and for values of the temperature and cross-interaction energy corresponding to state points in the homogeneous phase and in the limit of strong segregation. In the strongly segregated case, the system forms a spherical micellar phase, with the A- and B-blocks forming respectively the micellar coronas and cores. The parameters of the model have been selected in order to induce a much slower intrinsic mobility of the B-homopolymer in comparison to the A-homopolymer. In such conditions, the interplay between a strong interfacial barrier suppressing diffusion and a highly mobile surrounding corona induces a soft confinement effect on the B-blocks at the spherical cores. By introducing adequate correlators we have confirmed a strong internal mobility of the micellar interfaces in the present model.

We have characterized dynamic features by computing monomer displacements, end-to-end and bond reorientations, as well as relaxation of chain normal modes. Inspection of dynamic correlators reveals a shift of the intermediate time scales of the A- and B-homopolymers to respectively longer and shorter times for the blocks in the micellar phase. This effect is spectacular for the B-blocks, for which intermediate time scales are faster than in the B-homopolymer by many orders of magnitude. Having said this, a plateau regime arises at long-times in the micellar phase, which is associated with the mentioned suppression of motion induced by interfacial effects.

We have investigated the effect of several sources of dynamic heterogeneity in the averaged profiles exhibited by the computed correlators. Even with a very broad distribution of aggregation numbers, polydispersity in the core size has, as much, a moderate effect on dynamic heterogeneity. A very different effect has been found for the specific location of the bonds along the chain. The latter induces extreme differences between the time scales for reorientation of the bonds close to the interface and of those close to the chain ends.

We have computed Rouse normal modes for the B-block. In this way we implicitly assume that the effect of the coupling to the A-block and of the interactions with the other surrounding chains enters as an effective contribution to the friction coefficient and the set of stochastic forces introduced by the Rouse model. As observed for the dynamic observables mentioned above, the Rouse correlators for the B-block in the micellar phase exhibit a long-time plateau associated with interfacial effects. Still, scaling laws predicted by the Rouse model are fulfilled at time scales not probing the interface. The comparison of Rouse normal modes for the B-component in the diblock system and in the homopolymer state reveals scaling behavior. We propose to rationalize this feature within the Rouse model, for time scales not probing the interface, through an effective friction which depends on the temperature and the energy scale of the A$-$B interaction.

Acknowledgment. We acknowledge financial support from the projects NMP3-CT-2004-502235 (SoftComp, EU), MAT2007-63681 (Spain), 2007-60I021 (Spain), and IT-436-07

(GV, Spain). We thank M. Monkenbusch, D. Richter, and L. Willner for useful discussions and especially R. Lund for a critical reading of the manuscript.

References and Notes

(1) Bates, F. S.; Fredrickson, G. H. *Annu. Rev. Phys. Chem.* **1990**, *41*, 525.
(2) Bates, F. S. *Science* **1991**, *251*, 898.
(3) Fredrickson, G. H.; Bates, F. S. *Annu. Rev. Mat. Sci.* **1996**, *26*, 501.
(4) Alexandridis, P., Lindman, B., Eds. *Amphiphilic Block Copolymers*; Elsevier: Amsterdam, The Netherlands, 2000.
(5) Hamley, I. W. *Block Copolymers in Solution*; John Wiley & Sons: Chichester, U.K., 2005.
(6) Lodge, T. P. *Macromol. Chem. Phys.* **2003**, *204*, 265.
(7) Matsen, M. W.; Bates, F. S. *Macromolecules* **1996**, *29*, 1091.
(8) Matsen, M. W. *J. Phys.: Condens. Matter* **2002**, *14*, R21.
(9) Castelletto, V.; Hamley, I. W. *Curr. Opin. Solid State Mater. Sci.* **2004**, *8*, 426.
(10) Hajduk, D. A.; Harper, P. E.; Gruner, S. M.; Honeker, C. C.; Kim, G.; Thomas, E. L.; Fetters, L. J. *Macromolecules* **1994**, *27*, 4063.
(11) Hamley, I. W. *Nanotechnology* **2003**, *14*, R39.
(12) Binder, K.; Müller, M. *Curr. Opin. Colloid Interface Sci.* **2000**, *5*, 315.
(13) Colby, R. H. *Curr. Opin. Colloid Interface Sci.* **1996**, *1*, 454.
(14) Anastasiadis, S. H. *Curr. Opin. Colloid Interface Sci.* **2000**, *5*, 324.
(15) Papadakis, C. M.; Rittig, F. *J. Phys.: Condens. Matter* **2005**, *17*, R551.
(16) Yokoyama, H. *Mater. Sci. Eng. Res.* **2006**, *53*, 199.
(17) Yao, M.-L.; Watanabe, H.; Adachi, K.; Kotaka, T. *Macromolecules* **1991**, *24*, 2955.
(18) Ehlich, D.; Takenaka, M.; Hashimoto, T. *Macromolecules* **1993**, *26*, 492.
(19) Dalvi, M. C.; Eastman, C. E.; Lodge, T. P. *Phys. Rev. Lett.* **1993**, *71*, 2591.
(20) Dalvi, M. C.; Lodge, T. P. *Macromolecules* **1993**, *26*, 859.
(21) Haliloglu, T.; Balaji, R.; Mattice, W. L. *Macromolecules* **1994**, *27*, 1473.
(22) Lodge, T. P.; Dalvi, M. C. *Phys. Rev. Lett.* **1995**, *75*, 657.
(23) Ko, M. B.; Mattice, W. L. *Macromolecules* **1995**, *28*, 6871.
(24) Karatasos, K.; Anastasiadis, S. H.; Floudas, G.; Fytas, G.; Pispas, S.; Hadjichristidis, N.; Pakula, T. *Macromolecules* **1996**, *29*, 1326.
(25) Hoffmann, A.; Sommer, J. U.; Blumen, A. *J. Chem. Phys.* **1997**, *106*, 6709.
(26) Pakula, T.; Karatasos, K.; Anastasiadis, S. H.; Fytas, G. *Macromolecules* **1997**, *30*, 8463.
(27) Hamersky, M. W.; Tirrell, M.; Lodge, T. P. *Langmuir* **1998**, *14*, 6974.
(28) Murat, M.; Grest, G. S.; Kremer, K. *Europhys. Lett.* **1998**, *42*, 401.
(29) Murat, M.; Grest, G. S.; Kremer, K. *Macromolecules* **1999**, *32*, 595.
(30) Anastasiadis, S. H.; Rittig, F.; Chrissopoulou, K.; Fleischer, G.; Fytas, G.; Semenov, A. N.; Kärger, J.; Xenidou, M.; Pispas, S.; Hadjichristidis, N. *Europhys. Lett.* **2000**, *51*, 68.
(31) Rittig, F.; Kärger, J.; Papadakis, C. M.; Fleischer, G.; Almdal, K.; Štěpánek, P. *Macromolecules* **2001**, *34*, 868.
(32) Lorthioir, C.; Auroy, P.; Deloche, B.; Gallot, Y. *Eur. Phys. J. E* **2002**, *7*, 261.
(33) Lorthioir, C.; Alegría, A.; Colmenero, J.; Deloche, B. *Macromolecules* **2004**, *37*, 7808.
(34) Müller, M.; Daoulas, K. C. *J. Chem. Phys.* **2008**, *129*, 164906.
(35) Hamersky, M. W.; Hillmyer, M. A.; Tirrell, M.; Bates, F. S.; Lodge, T. P.; von Meerwall, E. D. *Macromolecules* **1998**, *31*, 5363.
(36) Cavicchi, K. A.; Lodge, T. P. *Macromolecules* **2004**, *37*, 6004.
(37) Khanna, V.; Kim, B. J.; Hexemer, A.; Mates, T. E.; Kramer, E. J.; Li, X.; Wang, J.; Hahn, S. F. *Macromolecules* **2007**, *40*, 2443.
(38) Hoffmann, A.; Sommer, J. U.; Blumen, A. *J. Chem. Phys.* **1997**, *107*, 7559.
(39) Yokoyama, H.; Kramer, E. J. *Macromolecules* **1998**, *31*, 7871.
(40) Fleischer, G.; Rittig, F.; Kärger, J.; Papadakis, C. M.; Mortensen, K.; Almdal, K.; Štěpánek, P. *J. Chem. Phys.* **1999**, *111*, 2789.
(41) Yokoyama, H.; Kramer, E. J. *Macromolecules* **2000**, *33*, 954.
(42) Yokoyama, H.; Kramer, E. J.; Fredrickson, G. H. *Macromolecules* **2000**, *33*, 2249.
(43) Papadakis, C. M.; Almdal, K.; Mortensen, K.; Rittig, F.; Fleischer, G.; Štěpánek, P. *Eur. Phys. J. E* **2000**, *1*, 275.
(44) Cavicchi, K. A.; Lodge, T. P. *Macromolecules* **2003**, *36*, 7158.
(45) Papadakis, C. M.; Rittig, F.; Almdal, K.; Mortensen, K.; Štěpánek, P. *Eur. Phys. J. E* **2004**, *15*, 359.
(46) Lund, R.; Willner, L.; Alegría, A.; Colmenero, J.; Richter, D. *Macromolecules* **2008**, *41*, 511.
(47) Kremer, K.; Grest, G. S. *J. Chem. Phys.* **1990**, *92*, 5057.
(48) Frenkel, D.; Smit, B. *Understanding Molecular Simulation*; Academic Press (Elsevier): San Diego, CA, 1996.
(49) Anderson, J. A.; Lorenz, C. D.; Travesset, A. *J. Chem. Phys.* **2008**, *128*, 184906.
(50) Boyd, R. H.; Gee, R. H.; Han, J.; Jin, Y. *J. Chem. Phys.* **1994**, *101*, 788.
(51) Boyd, S. U.; Boyd, R. H. *Macromolecules* **2001**, *34*, 7219.
(52) Doi, M.; Edwards, S. F. *The Theory of Polymer Dynamics*; Oxford University Press: Oxford, U.K., 1986.
(53) Teraoka, I. *Polymer Solutions*; John Wiley & Sons: New York, 2002.
(54) Kreer, T.; Baschnagel, J.; Müller, M.; Binder, K. *Macromolecules* **2001**, *34*, 1105.
(55) Ramos, J.; Vega, J. F.; Theodorou, D. N.; Martínez-Salazar, J. *Macromolecules* **2008**, *41*, 2959.
(56) Bennemann, C.; Baschnagel, J.; Paul, W.; Binder, K. *Comput. Theor. Polym. Sci.* **1999**, *9*, 217.
(57) Moreno, A. J.; Colmenero, J. *Phys. Rev. Lett.* **2008**, *100*, 126001.
(58) Kremer, K.; Grest, G. S.; Carmesin, I. *Phys. Rev. Lett.* **1988**, *61*, 566.
(59) Shaffer, J. S. *J. Chem. Phys.* **1995**, *103*, 761.
(60) Padding, J. T.; Briels, W. J. *J. Chem. Phys.* **2002**, *117*, 925.
(61) Brodeck, M.; Alvarez, F.; Moreno, A. J., Colmenero, J.; Richter, D. Submitted for publication.